

Research Article

Kupffer Phase Radiomics Signature in Sonazoid-Enhanced Ultrasound is an Independent and Effective Predictor of the Pathologic Grade of Hepatocellular Carcinoma

Chen Li ¹, Jingyong Xu ², Yuan Liu,¹ Mingxiao Wu,¹ Weide Dai,¹ Jinghai Song,² and Hanzhang Wang³

¹Department of Ultrasound, Beijing Hospital, National Centre of Gerontology, Institute of Geriatric Medicine, Chinese Academy of Medical Sciences, Beijing, China

²Department of General Surgery and Hepato-Bilio-Pancreatic Surgery, Beijing Hospital, National Centre of Gerontology, Institute of Geriatric Medicine, Chinese Academy of Medical Sciences, Beijing, China

³GE Healthcare, Shanghai, China

Correspondence should be addressed to Chen Li; lichen4525@bjhmoh.cn

Received 21 March 2022; Revised 25 May 2022; Accepted 27 May 2022; Published 27 June 2022

Academic Editor: Alessandro Granito

Copyright © 2022 Chen Li et al. This is an open access article distributed under the Creative Commons Attribution License, which permits unrestricted use, distribution, and reproduction in any medium, provided the original work is properly cited.

We conduct this study to investigate the value of Kupffer phase radiomics signature of Sonazoid-enhanced ultrasound images (SEUS) for the preoperative prediction of hepatocellular carcinoma (HCC) grade. From November 2019 to October 2021, 68 pathologically confirmed HCC nodules from 54 patients were included. Quantitative radiomic features were extracted from grayscale images and arterial and Kupffer phases of SEUS of HCC lesions. Univariate logistic regression and the maximum relevance minimum redundancy (MRMR) method were applied to select radiomic features best corresponding to pathological results. Prediction radiomic signature was calculated using each of the image types. A predictive model was validated using internal leave-one-out cross validation (LOOCV). For discrimination between poorly differentiated HCC (p-HCC) and well-differentiated HCC/moderately differentiated HCC (w/m-HCC), the Kupffer phase radiomic score (KPRS) achieved an excellent area under the curve (AUC = 0.937), significantly higher than the other two radiomic signatures. KPRS was the best radiomic score based on the highest AUC (AUC = 0.878), which is prior to gray and arterial RS for differentiation between w-HCC and m/p-HCC. Univariate and multivariate analysis incorporating all radiomic signatures and serological variables showed that KPRS was the only independent predictor in both predictions of HCC lesions (p-HCC vs. w/m-HCC, log OR 15.869, $P < 0.001$, m/p-HCC vs. w-HCC, log OR 12.520, $P < 0.05$). We conclude that radiomics signature based on the Kupffer phase imaging may be useful for identifying the histological grade of HCC. The Kupffer phase radiomic signature may be an independent and effective predictor in discriminating w-HCC and p-HCC.

1. Introduction

Liver cancer is the sixth most common malignancy and the fourth most common cause of cancer-related death worldwide [1]. Hepatocellular carcinoma (HCC) represents primary liver cancer and is the second leading cancer-related mortality in China [2]. Clinically, the development of HCC is prone to metastasis and recurrence, which limits the prognosis as well as the quality of life [3]. Pathological grading is associated with intrahepatic recurrence [3]. High-

grade HCC tumors have a higher risk of intrahepatic recurrence than low-grade tumors [4]. Accurate prediction of the HCC grade of differentiation might formulate the treatment strategy and predict the therapeutic outcome, prognosis, and risk of tumor recurrence [5, 6].

Medical radiological imaging is integral to the routine clinical method of patients with HCC. Radiomics is a technology that extract the characteristics of radiological image quantitatively [7]. Conventional imaging evaluation provides few metrics without tumor heterogeneity

information through the manual assessment of lesions by radiologists [8]. With the development of medical imaging data, radiomics are used to deeply excavate the biological characteristics of tumor imaging, quantitatively analyze tumor heterogeneity, and integrally evaluate tumor phenotype, which may be beyond conventional techniques. In fact, recent studies have developed that pathological grading is related to the radiomics algorithm acquired from magnetic resonance imaging (MRI) or computed tomography (CT), such as prediction of a pathological grade of gliomas and renal carcinoma [9, 10].

Compared with CT and MRI, ultrasound (US) is simple, radiation-free, inexpensive, and commonly used to monitor the liver lesions [11]. Contrast-enhanced ultrasound score (CEUS) can observe the real-time vascular phase with microcirculation perfusion information. The microbubbles of a contrast agent called Sonazoid can be phagocytosed by Kupffer cells, which rarely exist in tumors, and then Sonazoid-enhanced US (SEUS) provides a special phase called the Kupffer phase or the post-vascular phase [12, 13]. Previous studies have reported that the degree of the contrast defect in the Kupffer phase are related to histological grading of HCC, and certain quantifiable patterns of CEUS were associated with treatment outcomes [14–16].

To better interpret SEUS, we have, therefore, developed radiomics for evaluating the histological grading of HCC based on US, arterial phase, and Kupffer-phase by SEUS. Our study aims to evaluate the feasibility of US and SEUS radiomics models in terms of differentiation histologically grades of HCC to determine an initial prognosis of HCC.

2. Materials and Methods

2.1. Patients. The institutional review board of our institution approved this retrospective study and waived the requirement to obtain written informed consent. Figure 1 shows the enrolment of patients.

Between November 2019 and October 2021, 71 consecutive patients with HCC were retrospectively recruited. Inclusion criteria were as follows: (1) grayscale ultrasound image and SEUS were performed preoperatively in each patient; (2) no prior surgical or medical treatment was administered for the suspected HCC lesions; (3) the diagnoses of HCC were obtained by US/CT-guided percutaneous biopsy and surgical resection. Exclusion criteria were as follows: (1) patients without SEUS; (2) patients with previous treatment (i.e., radiofrequency ablation or transarterial chemoembolization) before ultrasound imaging; (3) patients without available histological report; (4) unclear or unsatisfied grayscale or SEUS images of focal liver lesions. A total of 54 patients with 68 histologically confirmed HCC nodules were enrolled in this study. The clinical characteristics of patients contain age, gender, tumor maximum diameter, alpha-fetoprotein (AFP) values, total bilirubin (TBil), direct bilirubin (DBil), carbohydrate antigen 12-5 (CA12-5), carbohydrate antigen 19-9 (CA19-9), carbohydrate antigen 15-3 (CA15-3),

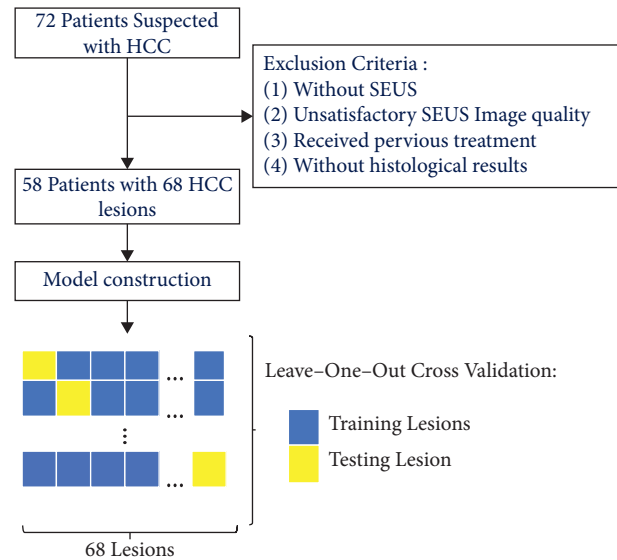


FIGURE 1: Flowchart of the study.

aspartate transaminase (AST), and alanine transaminase (ALT).

2.2. Assessment of Pathological Grade. Among 54 patients with 68 HCC nodules, the diagnosis was confirmed by pathological examination of specimens obtained by US/CT-guided percutaneous biopsy ($n = 28$) and surgical resection ($n = 41$). Histological grade of HCC tumors was obtained by the pathologist. According to the International Working Party Classification, the degree of differentiation was determined [7]. Histological grade included well-differentiated HCC (w-HCC, $n = 12$, 17.4%), moderately differentiated HCC (m-HCC, $n = 41$, 59.4%), and poorly differentiated HCC (p-HCC, $n = 15$, 21.7%).

2.3. Contrast-Enhanced Ultrasound Imaging. All patients underwent conventional ultrasound in B-mode and SEUS by two sonographers with more than 5 years of experience in standard liver CEUS. All SEUS was performed by two sonographers using Aplio 500 (Canon, Honshu, Japan) with a convex probe (6C1, 1–6 MHz) and a linear probe (11L4, 4–11 MHz) and Aplio i800 (Canon, Honshu, Japan) with a convex probe (PVI-475BX, 1–8 MHz) and a linear probe (11L4, 4–11 MHz). The mechanical index (MI) for the acoustic output was set to 0.19–0.22 and the dynamic range was 65–70 dB according to the size of the lesion. Patients received a bolus intravenous injection of Sonazoid (perfluorobutane, GE Healthcare, Oslo, Norway) through a peripheral venous line, followed by 5 mL of normal saline flush. Immediately after the administration of Sonazoid, the hepatic arterials, portal veins, hepatic veins, and the normal liver parenchyma were uniformly enhanced during an early vascular phase image lasting 3 minutes. Approximately 10 minutes after injection, the liver was scanned again to observe the post-vascular phase image (Kupffer phase). The arterial phase and the Kupffer phase were obtained by scanning 15 to 30 seconds and 15 minutes, respectively.

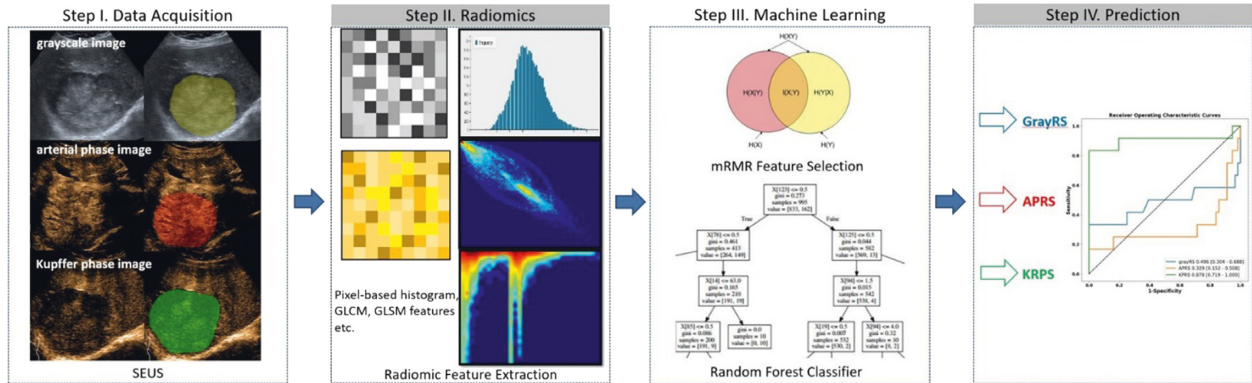


FIGURE 2: Radiomics analysis. SEUS, Sonazoid-enhanced ultrasound; grayRS, grayscale radiomic score (grayRS); APRS, arterial phase radiomic score; KPRS, Kupffer phase radiomic score.

2.4. Image Segmentation. Image segmentation was performed on grayscale, arterial phase, and Kupffer phase retrieved from DICOM (Digital Imaging and Communications in Medicine) format files. The images were loaded into the ITK-SNAP software (open-source software, <https://www.itksnap.org>) for manual segmentation, and a three-dimensional volume of interest (VOI) that covered the whole tumor was delineated in the images, respectively, segmented by a sonographer with over five years of experience in abdominal CEUS imaging. The procedure is shown in Figure 1 and details are introduced as follows.

2.5. Radiomics Analysis. After integrating VOI that covered the whole tumor images, a three-dimensional radiomics feature was extracted from grayscale, arterial phase, and Kupffer phase images using the NUK software (novo ultrasound kit, GE Healthcare Shanghai, China). Specifically, shape-based ($n=9$), first-order ($n=18$), gray-level cooccurrence matrix (GLCM, $n=24$), gray-level dependency matrix (GLDM, $n=14$), gray-level run-length matrix (GLRLM, $n=16$), gray level size zone matrix (GLSZM, $n=16$), and neighbouring gray tone difference matrix (NGTDM, $n=5$) features, according to the imaging biomarker standardization initiative from both original images and filter derived images were extracted. SMOTE up- and down-sampling was applied to create a balanced training dataset, which had been used in other radiomic studies.

Z-score normalization was applied to radiomic features. Each radiomic feature's association with the outcome (pathologically confirmed HCC differentiation status) were initially assessed using univariate logistic analysis. Radiomic features significant in univariate analysis were further selected using maximum relevance minimum redundancy (MRMR) to obtain 15 features most contributing to the outcome with least correlation. The final prediction of the outcome was obtained by a random forest classifier (RFC) trained on selected radiomic features, in the form of a radiomic score per lesion, which was calculated by linear combination of radiomic features with associated weights.

The univariate-multivariate logistic model with an adjusted odds ratio (OR) was constructed using the radiomic score calculated from grayscale radiomic score (grayRS),

arterial phase radiomic score (APRS), and Kupffer phase radiomic score (KPRS) images. Different HCC differentiations (low, medium, and high) were analyzed using “one versus rest” strategy (OvR).

Radiomic scores and the model's discrimination ability of pathological HCC differentiation were characterized using receiver operation characteristic (ROC) analysis; the area under the curve (AUC) was used to quantify model performance. Predictive performances including accuracy, sensitivity, and specificity of the predictors were calculated at the optimal decision boundary on the ROC curve determined by maximizing the Youden's index. Leave-one-out cross validation (LOOCV) was applied for model validation (Figure 2).

2.6. Statistical Analysis. Descriptive statistics were presented in mean with standard deviation or median with interquartile range depending on variables' normality. The Shapiro-Wilk test was used to assess normality. 95% Confidence intervals for model evaluation were calculated using the bootstrap method with 1000 random resamples. The DeLong test was used to compare AUC differences. The McNemar Chi-squared test was used to compare predictive performances. The Hosmer-Lemeshow test was used to assess significance of model's deviation from perfect fit. Variables significant in univariate analysis were passed to multivariate analysis. A two-sided P value less than 0.05 was considered statistically significant.

3. Results

3.1. Patient Characteristics. In total, 54 patients were included containing 48 males and 6 females, with a mean age of 61.5 years (range from 41 to 88 years). Sixty-eight lesions were detected and studied among 54 HCC patients. Most of the patients had a history of chronic liver disease and cirrhosis, including hepatitis C virus (HCV) infection in 1 patient (1.9%), hepatitis B virus (HBV) infection in 43 patients (79.6%), HCV and HBV infection in 3 patients (5.6%), nonalcoholic steatohepatitis (NASH) in 7 patients (13%), and cirrhosis in 40 patients (74.1%). The median total bilirubin and direct bilirubin were 14.70

TABLE 1: Prediction performance on p-HCC versus w/m-HCC.

Radiomic score	AUC	Accuracy	Sensitivity	Specificity
grayRS	0.555 (0.368, 0.733)	66.2% (55.9%, 75.0%)	46.7% (23.8%, 66.7%)	71.7% (60.4%, 81.5%)
APRS	0.349 (0.170, 0.539)	79.4% (72.1%, 86.8%)	13.3% (0.00%, 30.0%)	98.1% (94.4%, 100.0%)
KPRS	0.937 (0.821, 1.000)	97.1% (92.6%, 100.0%)	93.3% (80.0%, 100.0%)	98.1% (94.6%, 100.0%)

grayRS: grayscale radiomic score; APRS: arterial phase radiomic score; KPRS: Kupffer phase radiomic score.

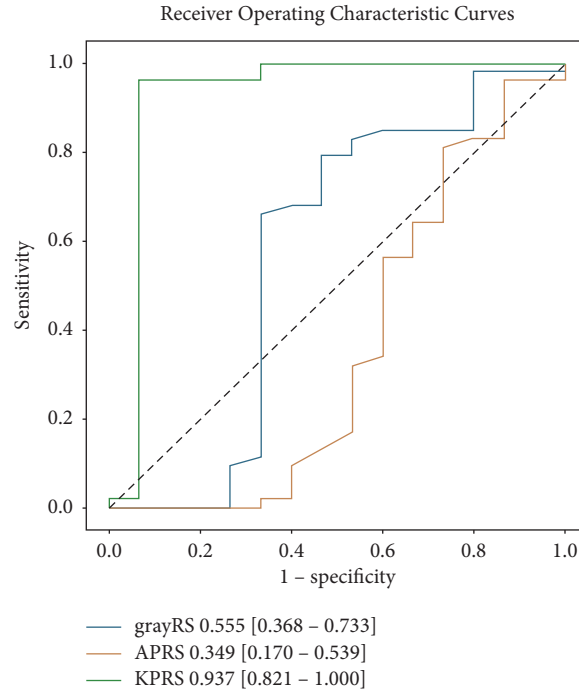


FIGURE 3: ROC curves of radiomic features: the differentiation between p-HCC and w/m-HCC.

TABLE 2: Univariate analysis and multivariate analysis for p-HCC versus w/m-HCC.

Variables	Univariate				Multivariate			
	log (OR)	(0.025	0.975)	P	log (OR)	(0.025	0.975)	P
AFP	0.000	0.000	0.000	1.000				
TBil	0.001	-0.007	0.009	0.788				
DBil	0.000	-0.007	0.008	0.951				
AST	0.004	0.000	0.010	0.263				
ALT	0.005	-0.003	0.012	0.195				
CA125	-0.001	-0.005	0.002	0.451				
CA19-9	0.003	-0.007	0.013	0.606				
CA153	-0.011	-0.061	0.040	0.671				
grayRS	0.145	-4.763	5.054	0.954				
APRS	-6.533	-11.339	-1.728	0.023	-9.132	-18.686	0.422	0.061
KPRS	14.940	7.313	22.567	<0.001	15.869	7.218	24.520	<0.001
const.					-1.363	-3.693	0.968	0.252

AFP, alpha-fetoprotein; TBil, total bilirubin; DBil, direct bilirubin; AST, aspartate transaminase; ALT, alanine transaminase; CA, carbohydrate antigen; grayRS, grayscale radiomic score; APRS, arterial phase radiomic score; KPRS, Kupffer phase radiomic score; const., constant.

(10.00–21.20) and 5.00 (3.70–7.80) $\mu\text{mol/L}$, respectively. ALT was 24.00 (17.75–49.75) and AST was 30.00 (21.00–55.50) U/L. Some of the tumor markers were recorded, such as AFP 5.90 (2.85–122.45) $\mu\text{g/L}$, CA19-9 8.75 (3.92–17.15) U/ml, CA125 14.35 (9.47–30.93) U/ml, and CA153, 8.70 (6.65–11.93) U/ml.

3.2. Differentiation of w/m-HCCs from p-HCCs. At the task of differentiating w/m-HCC from p-HCC lesions, radiomic scores calculated from grayRS and APRS displayed poor if not no discrimination abilities based on ROC analysis. KPRS showed an excellent AUC of 0.937 (95% confidence interval (CI): 0.821, 1.000), significantly higher than the other two

TABLE 3: Prediction performance on w-HCC versus m/p-HCC.

Radiomic score	AUC	Accuracy	Sensitivity	Specificity
GrayRS	0.496 (0.304, 0.688)	85.3% (77.9%, 91.2%)	25.0% (7.1%, 45.5%)	98.2% (94.7%, 100.0%)
APRS	0.329 (0.152, 0.508)	82.4% (75.0%, 89.7%)	16.7% (0.00%, 35.7%)	96.4% (92.5%, 100.0%)
KPRS	0.878 (0.719, 1.000)	97.1% (92.6%, 100.0%)	83.3% (62.5%, 100.0%)	100.0% (100.0%, 100.0%)

grayRS: grayscale radiomic score; APRS: arterial phase radiomic score; KPRS: Kupffer phase radiomic score.

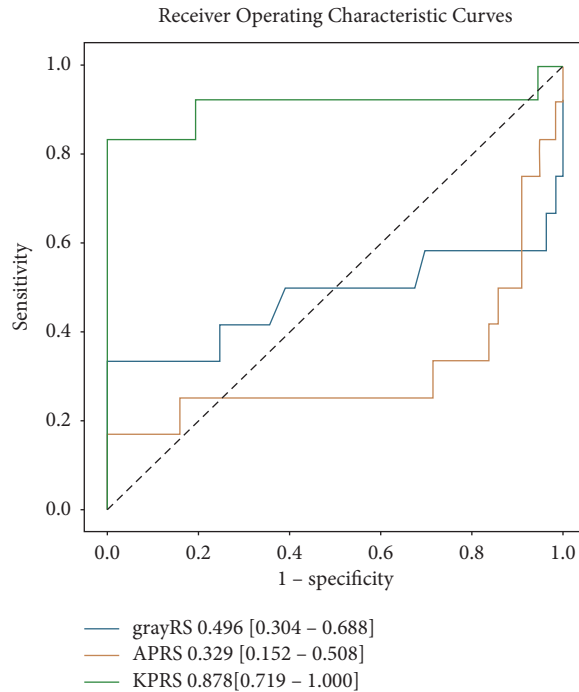


FIGURE 4: ROC curves of radiomic features: the differentiation between w-HCC and m/p-HCC.

TABLE 4: Univariate analysis and multivariate analysis m/p-HCC versus w-HCC.

Variables	Univariate				Multivariate			
	log (OR)	(0.025	0.975)	P	log (OR)	(0.025	0.975)	P
AFP	0.000	0.000	0.000	1				
TBil	0.009	-0.005	0.023	0.224				
DBil	0.009	-0.006	0.023	0.226				
AST	-0.001	0.007	0.004	0.641				
ALT	-0.003	-0.010	0.003	0.327				
CA125	0.000	-0.006	0.005	0.86				
CA199	0.016	0.004	0.029	0.007	0.011	-0.009	0.031	0.269
CA153	0.009	-0.045	0.063	0.755				
grayRS	-3.165	-8.381	2.052	0.234				
APRS	-1.813	-4.792	1.166	0.233				
KPRS	14.454	7.154	21.753	<0.001	12.520	5.333	19.707	0.017
const.					-11.093	-17.036	-5.151	<0.001

AFP, alpha-fetoprotein; TBil, total bilirubin; DBil, direct bilirubin; AST, aspartate transaminase; ALT, alanine transaminase; CA, carbohydrate antigen; grayRS, gray scale radiomic score; APRS, arterial phase radiomic score; KPRS, Kupffer phase radiomic score; const., constant.

radiomic scores (All DeLong test $P < 0.05$). KPRS achieved an accuracy, sensitivity, and specificity of 97.1% (95% CI: 92.6%, 100%), 93.3% (80.0%, 100%), and 98.1% (94.6%, 100%), respectively (Table 1, Figure 3).

Univariate analysis showed that no serological variables were significantly related to p-HCC and w/m-HCC

(Table 2). APRS (log OR -6.533 , 95% CI $(-11.339, -1.728)$, $P < 0.05$) and KPRS (log OR 14.940 , 95% CI $(7.313, 22.567)$, $P < 0.001$) showed significance in univariate analysis, but only KPRS demonstrated to be an independent predictor in multivariate analysis (log OR 15.869 , 95% CI $(7.218, 24.520)$, $P < 0.001$).

3.3. Differentiation of w-HCC from m/p-HCC. KPRS was the best radiomic score based on the highest AUC: 0.878 (95% CI: 0.719, 1.000). KPRS also showed excellent predictive performance (Table 3, Figure 4) with a sensitivity of 83.3% and specificity of 100%. As a comparison, grayRS and APRS displayed AUC lower than 0.5, which was considered poor performance.

Univariate analysis showed that CA19-9 (log OR 0.016, 96% CI (0.004, 0.029), $P < 0.05$) and KPRS (log OR 14.454, 95% CI 7.154, 21.753), $P < 0.001$) were significant predictors for differentiation w-HCC from m/p-HCC (Table 4). KPRS (log OR 12.520, 95% CI (5.333, 19.707), $P < 0.05$) was the only independent predictor in multivariate analysis. KPRS was sufficient at discriminating w-HCC and m/p-HCC.

4. Discussion

Radiomics is a noninvasive technology based on the quantitative extraction of signature from radiological imaging modalities [7]. In fact, investigators have shown that radiomics may be useful for predicting progression-free and overall survival for malignant diseases [17, 18]. Recently, radiomics analysis based on ultrasound imaging technology has achieved some good results in the early diagnosis, prognosis, and prediction of diseases.

CEUS is widely used to observe microcirculation blood perfusion of liver cancer [19]. We used the radiomics method to evaluate the overall information related to the difference of grade that maybe contained in tumors by extracting multiphase CEUS imaging features. Therefore, the aim of our study was to develop and validate CEUS radiomics models based on US, arterial phase and Kupffer-phase for predicting the histological grading of HCC. Our study showed that for discrimination between p-HCC and w/m-HCC, KPRS showed an excellent AUC of 0.937, significantly higher than grayRS and APRS. Meanwhile, KPRS was the best radiomic score based on the highest AUC (AUC = 0.878), which is prior to grayRS and APRS for the differentiation between w-HCC and m/p-HCC. Wu et al. investigated MRI-based radiomics signatures for the HCC grade, and the AUC of model using radiomics signatures was 0.742 [20]. Our study showed that the prediction model using radiomics signatures based on KPRS (AUC = 0.937, 0.878) is prior to MRI, which means KPRS had advantages in predicting the HCC grade. The easy-to-use graphic tool might provide important characteristics to stimulate clinical prediction. Therefore, our study had potential application of SEUS in the diagnosis of focal liver lesions than conventional contrast medium and CT [21]. Moreover, with the number of focal liver lesions increased in HCC and other kind of tumor prior to different subtypes of hepatocellular adenoma [22].

Our study demonstrated that only KPRS demonstrated to be an independent predictor in univariate analysis and multivariate analysis in predicting the HCC grade. On the other hand, KPRS showed a better discrimination performance compared with the combination of clinical risk factors and KPRS, while, the results of were inconsistent with the previous studies. Wu et al. showed that the combination

of MRI radiomics signatures with clinical factors could be useful for discriminating between high-grade and low-grade HCC, and both the AFP level and radiomics signatures were independent predictors [20]. Mohamed et al. demonstrated that serological markers, such as serum vitronectin and AFP, speculated a potential role in diagnosis and prognosis of HCC [23]. This is, probably, because of the different classification of pathological grade and the number of cases, HCC tumors were divided into low-grade and high-grade cases instead of using the International Working Party Classification or the Edmondson grade.

Limitations of this study should be acknowledged. First, the number of HCC cases was relatively limited, and HCC tumors were divided into well, moderate, and poorly differentiate-cases, while no ideal results were obtained discriminating between m-HCC and rest. Second, our study was performed in a single center, further multicenter cohorts might be necessary to evaluate the reliability, and to verify the generalizability of our findings. Third, the potential use of SEUS combined with gadoteric acid-enhanced magnetic resonance may provide more characteristics to increase prediction [24]. In the future, multimodality ultrasound imaging-including color Doppler-flow imaging, ultrasound elastography, and vascular phase of CEUS imaging-will be combined to improve the performance of HCC classification.

5. Conclusions

In conclusion, radiomics signatures based on the Kupffer phase imaging may be useful for identifying the histological grade of HCC. Additionally, the Kupffer phase radiomic signature may be an independent and effective predictor in discriminating w-HCC and p-HCC.

Data Availability

The data that support the findings of this study are available from the corresponding author upon reasonable request.

Ethical Approval

This study was approved by the Ethics Committee of the Beijing Hospital (2021BJYYEC-190-02).

Conflicts of Interest

The authors declare that they have no conflicts of interest.

Authors' Contributions

Conception and design were performed by JY Xu and C Li. Administrative support was performed by C Li, JH Song, and WD Dai. Provision of study materials or patients was done by JY Xu, Y Liu, and MX Wu. Collection and assembly of data were performed by JY Xu, Y Liu, and MX Wu. Data analysis and interpretation were performed by JY Xu, Y Liu, MX Wu, C Li, and HZ Wang. Manuscript writing was done by all the authors. Final approval of manuscript was given by all the authors.

Acknowledgments

The authors appreciate our colleagues from the departments of oncology, ultrasound, and surgery for their contributions to case collection, transfer, and follow-up. The authors thank Miss Jingjing Xia for her technical support in radiomics analysis. This study was supported by Beijing Hospital Project (No. BJ-2021-187).

References

- [1] F. Bray, J. Ferlay, I. Soerjomataram, R. L. Siegel, L. A. Torre, and A. Jemal, "Global cancer statistics 2018: GLOBOCAN estimates of incidence and mortality worldwide for 36 cancers in 185 countries," *CA: A Cancer Journal for Clinicians*, vol. 68, no. 6, pp. 394–424, 2018.
- [2] W. Chen, R. Zheng, P. D. Baade et al., "Cancer statistics in China, 2015," *CA: A Cancer Journal for Clinicians*, vol. 66, no. 2, pp. 115–132, 2016.
- [3] A. Sasaki, S. Kai, Y. Iwashita, S. Hirano, M. Ohta, and S. Kitano, "Microsatellite distribution and indication for locoregional therapy in small hepatocellular carcinoma," *Cancer*, vol. 103, no. 2, pp. 299–306, 2005.
- [4] I. O. L. Ng, E. C. S. Lai, S. T. Fan, M. M. T. Ng, and M. K. P. So, "Prognostic significance of pathologic features of hepatocellular carcinoma: a multivariate analysis of 278 patients," *Cancer*, vol. 76, no. 12, pp. 2443–2448, 1995.
- [5] S. Tamura, T. Kato, M. Berho et al., "Impact of histological grade of hepatocellular carcinoma on the outcome of liver transplantation," *Archives of Surgery*, vol. 136, no. 1, p. 25, 2001.
- [6] T. Kumada, S. Nakano, I. Takeda et al., "Patterns of recurrence after initial treatment in patients with small hepatocellular carcinoma," *Hepatology*, vol. 25, no. 1, pp. 87–92, 1997.
- [7] W. Hu, H. Yang, H. Xu, and Y. Mao, "Radiomics based on artificial intelligence in liver diseases: where we are?" *Gastroenterology Report*, vol. 8, no. 2, pp. 90–97, 2020.
- [8] W. L. Bi, A. Hosny, M. B. Schabath et al., "Artificial intelligence in cancer imaging: clinical challenges and applications," *CA: A Cancer Journal for Clinicians*, vol. 69, no. 2, 2019.
- [9] H. Y. Deng, J. Yang, T. F. Keng et al., "Diagnosis efficacy of MRI radiomics in grading of cerebral glioma before operation," *Radiologic Practice*, vol. 32, no. 12, pp. 1229–1233, 2017.
- [10] X. H. Li, Z. L. Fei, Y. P. Liu et al., "Value renal CT volumetric texture analysis with machine learning radiomics in assessment of pathological grade of clear cell renal cell carcinoma," *Chinese Journal of Radiology*, vol. 52, no. 5, pp. 344–348, 2018.
- [11] M. Ahmed, L. Solbiati, C. L. Brace et al., "Image-guided tumor ablation: standardization of terminology and reporting criteria—a 10-year update," *Radiology*, vol. 273, no. 1, pp. 241–260, 2014.
- [12] A. Alzaraa, G. Gravante, W. Y. Chung et al., "Contrast-enhanced ultrasound in the preoperative, intraoperative and postoperative assessment of liver lesions," *Hepatology Research: the Official Journal of the Japan Society of Hepatology*, vol. 43, no. 8, pp. 809–819, 2013.
- [13] C. Li, Y. Liu, J. Xu, J. Song, M. Wu, and J. Chen, "Contrast-enhanced intraoperative ultrasonography with Kupffer phase may change treatment strategy of metastatic liver tumors - a single-centre prospective study," *Therapeutics and Clinical Risk Management*, vol. 17, no. 17, pp. 789–796, 2021.
- [14] K. Korenaga, M. Korenaga, M. Furukawa, T. Yamasaki, and I. Sakaida, "Usefulness of Sonazoid contrast-enhanced ultrasonography for hepatocellular carcinoma: comparison with pathological diagnosis and superparamagnetic iron oxide magnetic resonance images," *Journal of Gastroenterology*, vol. 44, no. 7, pp. 733–741, 2009.
- [15] K. Sugimoto, F. Moriyasu, K. Saito et al., "Comparison of Kupffer-phase Sonazoid-enhanced sonography and hepatobiliary-phase gadoxetic acid-enhanced magnetic resonance imaging of hepatocellular carcinoma and correlation with histologic grading," *Journal of Ultrasound in Medicine*, vol. 31, no. 4, pp. 529–538, 2012.
- [16] R. H. Zou, Q. G. Lin, W. Huang et al., "Quantitative contrast-enhanced ultrasonic imaging reflects microvascularization in hepatocellular carcinoma and prognosis after resection," *Ultrasound in Medicine & Biology*, vol. 41, no. 10, pp. 2621–2630, 2015.
- [17] J. Lao, Y. Chen, Z. C. Li et al., "A deep learning-based radiomics model for prediction of survival in glioblastoma multiforme," *Scientific Reports*, vol. 7, no. 1, Article ID 10353, 2017.
- [18] B. Zhang, J. Tian, D. Dong et al., "Radiomics features of multiparametric MRI as novel prognostic factors in advanced nasopharyngeal carcinoma," *Clinical Cancer Research: An Official Journal of the American Association for Cancer Research*, vol. 23, no. 15, pp. 4259–4269, 2017.
- [19] C. F. Dietrich, C. P. Nolsoe, R. G. Barr et al., "Guidelines and good clinical practice recommendations for contrast-enhanced ultrasound (CEUS) in the liver—update 2020 WFUMB in cooperation with EFSUMB, AFSUMB, AIUM, and FLAUS," *Ultrasound in Medicine & Biology*, vol. 46, no. 10, pp. 2579–2604, 2020.
- [20] M. Wu, H. Tan, F. Gao et al., "Predicting the grade of hepatocellular carcinoma based on non-contrast-enhanced MRI radiomics signature," *European Radiology*, vol. 29, no. 6, pp. 2802–2811, 2019.
- [21] A. Forgiione, F. Tovoli, M. Ravaioli et al., "Contrast-enhanced ultrasound LI-RADS LR-5 in hepatic tuberculosis: case report and literature review of imaging features," *Gastroenterology Insights*, vol. 12, pp. 1–9, 2021.
- [22] C. Chálim Rebelo, D. B. Moura, M. Flor de Lima et al., "An extreme case of liver adenomatosis: are they all the same?" *Gastroenterology Insights*, vol. 13, no. 1, pp. 68–76, 2022.
- [23] S. Y. Mohamed, A. E. Esmail, M. A. Shabana, and N. F. Ibrahim, "Assessment of plasma vitronectin as diagnostic and prognostic marker of hepatocellular carcinoma in patients with hepatitis C virus cirrhosis," *Gastroenterology Insights*, vol. 13, no. 1, pp. 9–19, 2022.
- [24] A. Granito, M. Galassi, F. Piscaglia et al., "Impact of gadoxetic acid (Gd-EOB-DTPA)-enhanced magnetic resonance on the non-invasive diagnosis of small hepatocellular carcinoma: a prospective study," *Alimentary Pharmacology & Therapeutics*, vol. 37, no. 3, pp. 355–363, 2013.